



HHS Public Access

Author manuscript

Amino Acids. Author manuscript; available in PMC 2016 December 26.

Published in final edited form as:

Amino Acids. 2014 March ; 46(3): 701–715. doi:10.1007/s00726-013-1548-3.

Modulation of polyamine metabolic flux in adipose tissue alters the accumulation of body fat by affecting glucose homeostasis

Chunli Liu,

AHB/552, Department of Biochemistry, Temple University School of Medicine, 3307N. Broad Street, Philadelphia, PA 19140, USA

Oscar Perez-Leal,

AHB/552, Department of Biochemistry, Temple University School of Medicine, 3307N. Broad Street, Philadelphia, PA 19140, USA

Carlos Barrero,

AHB/552, Department of Biochemistry, Temple University School of Medicine, 3307N. Broad Street, Philadelphia, PA 19140, USA

Kamyar Zahedi,

Division of Nephrology and Hypertension, Department of Medicine, University of Cincinnati College of Medicine, Cincinnati, OH 45267-0585, USA

Manoocher Soleimani,

Division of Nephrology and Hypertension, Department of Medicine, University of Cincinnati College of Medicine, Cincinnati, OH 45267-0585, USA

Carl Porter, and

Grace Cancer Drug Center, Roswell Park Cancer Institute, Elm and Carlton Streets, Buffalo, NY 14263, USA

Salim Merali

AHB/552, Department of Biochemistry, Temple University School of Medicine, 3307N. Broad Street, Philadelphia, PA 19140, USA

Abstract

The continued rise in obesity despite public education, awareness and policies indicates the need for mechanism-based therapeutic approaches to help control the disease. Our data, in conjunction with other studies, suggest an unexpected role for the polyamine catabolic enzyme spermidine/spermine-N1-acetyltransferase (SSAT) in fat homeostasis. Our previous studies showed that deletion of SSAT greatly exaggerates weight gain and that the transgenic overexpression suppresses weight gain in mice on a high-fat diet. This discovery is substantial but the underlying molecular linkages are only vaguely understood. Here, we used a comprehensive systems biology approach, on white adipose tissue (WAT), to discover that the partition of acetyl-CoA towards

Correspondence to: Salim Merali.

Electronic supplementary material The online version of this article (doi:10.1007/s00726-013-1548-3) contains supplementary material, which is available to authorized users.

Conflict of interest The authors declare that they have no conflict of interest.

polyamine catabolism alters glucose homeostasis and hence, fat accumulation. Comparative proteomics and antibody-based expression studies of WAT in SSAT knockout, wild type and transgenic mice identified nine proteins with an increasing gradient across the genotypes, all of which correlate with acetyl-CoA consumption in polyamine acetylation. Adipose-specific SSAT knockout mice and global SSAT knockout mice on a high-fat diet exhibited similar growth curves and proteomic patterns in their WAT, confirming that attenuated consumption of acetyl-CoA in acetylation of polyamines in adipose tissue drives the obese phenotype of these mice. Analysis of protein expression indicated that the identified changes in the levels of proteins regulating acetyl-CoA consumption occur via the AMP-activated protein kinase pathway. Together, our data suggest that differential expression of SSAT markedly alters acetyl-CoA levels, which in turn trigger a global shift in glucose metabolism in adipose tissue, thus affecting the accumulation of body fat.

Keywords

Adipose tissue metabolism; SSAT; Polyamine acetylation; Polyamine catabolism

Introduction

The rising prevalence of obesity has become a major public health concern over the last decade (NCHS 2008). Obesity is associated with many life-threatening conditions, such as type II diabetes, stroke, cardiovascular disease, and certain types of cancer. The health risk of obesity is greatly reduced by even modest weight loss (i.e. 5 %). However, despite the broad use of weight control practices, few individuals manage to maintain significant weight loss. There is an urgent need to understand all of the physiological mechanisms that regulate fat deposition/mobilization. This study was designed to evaluate spermidine/spermine- N^1 -acetyltransferase (SSAT) as an important novel metabolic link between polyamine metabolism and adipose tissue lipogenesis.

Polyamines (putrescine, spermidine, and spermine) are small positively charged molecules found in all cells, including adipocytes. With rare exception, polyamines do not incorporate into macromolecules but bind electrostatically to negatively charged macromolecules, such as nucleic acids. Although the function of polyamines remains unclear, it is known that they are essential for cell growth (Pegg and McCann 1982; Wang and Casero 2006). Thus, their intracellular levels are carefully regulated by homeostatic interactions between the anabolic and catabolic components involved in their metabolism.

SSAT is the key enzyme in the catabolism of polyamines, as it catalyzes the transfer of acetyl groups from acetyl-coenzyme A (acetyl-CoA) onto the intracellular polyamines spermidine or spermine. This acetylation reduces the positive charges on these molecules, alters their binding activity with biological molecules and renders them susceptible to cellular excretion and/or catabolism (Pegg 2008). Importantly, it also alters their ability to activate homeostatic responses. In mammalian cells, SSAT is tightly regulated and highly inducible by polyamines and polyamine analogues, e.g., N^1, N^{11} di(ethyl)norspermine (DENSPM) (Fogel-Petrovic et al. 1996). The importance of SSAT in regulating polyamine

homeostasis is indicated by its very short half-life, in the order of 20 min, which allows the cell to rapidly change the enzyme and in polyamine levels (McCloskey and Pegg 2003).

Recently, the ability of SSAT to control flux through the metabolic pathway and in the case of overexpression, to lead to futile cycling was elucidated by Kramer et al. (2008). Further, our studies have shown that overexpression of SSAT in transgenic mice (SSAT-tg) increases energy expenditure, producing a polyamine-based cycle, reducing the levels of acetyl-CoA and malonyl-CoA, effect that leads to decreased fatty acid biosynthesis and increased fatty acid oxidation, respectively (Jell et al. 2007; Kramer et al. 2008; Pietila et al. 1997; Pirinen et al. 2007). We have also shown that deletion of SSAT in knockout mice (SSAT-ko) greatly exaggerates weight gain and that this event is associated with a reduction in acetyl-CoA consumption for polyamine acetylation, an increase in the acetyl-CoA pool, an increase in the malonyl-CoA pool, an increase in fatty acid synthesis, a decrease in oxidative phosphorylation and a marked increase in total body fat accumulation (Jell et al. 2007; Kramer et al. 2008; Pietila et al. 1997; Pirinen et al. 2007). Indirect calorimetry revealed a significant increase in the oxygen exchange rate and heat production, suggesting increased energy expenditure, an observation that is consistent with the decreased levels of malonyl-CoA in white adipose tissue (WAT) and increased fat oxidation in liver slices taken from SSAT transgenic mice (Jell et al. 2007). Based on these data, we postulated that the reduced consumption of acetyl-CoA in adipose tissue by polyamine acetylation leads to reduced calorie loss under physiological conditions and thus contributing to altered glucose and fat metabolism. To test our hypothesis, we performed a combination of proteomics, fluxomics, metabolomics and antibody-based expression studies on the white adipose tissue (WAT) of SSAT-ko, SSAT-wt and SSAT-tg mice. We also tested the role of adipose tissue in driving the obese phenotype. Together, our data reveal a novel mechanism by which SSAT is able to regulate WAT glucose homeostasis through the modulation of acetyl-CoA.

Materials and methods

Materials

The SSAT-tg and SSAT-ko mice were derived and provided by L. Alhonen (University of Eastern Finland, Kuopio, Finland). All reagents for 2-DE, including IPG strips, mineral oil, Bio-Lyte ampholytes pH 3–10, 30 % bis-acrylamide, *N,N,N,N*-tetramethylethylenediamine (TEMED), ammonium persulfate, glycine, Tris base, urea, 3-[(3-cholamidopropyl)dimethyl-ammonio]-1-propanesulfonate (CHAPS), and glycerol were purchased from Bio-Rad. SimplyBlue SafeStain was from Invitrogen. Mouse monoclonal antibodies against lamin A and β -actin and the horseradish peroxidase (HRP)-conjugated goat anti-mouse immunoglobulin secondary antibody were obtained from Santa Cruz Biotech. Rabbit monoclonal antibodies against AMPK α , phospho-AMPK α (Thr172), AMPK β 1/2, phospho-AMPK β 1, acetyl-CoA carboxylase (C83B10) and phospho-acetyl-CoA carboxylase (Ser79) were from Cell Signaling Technology. The manufacturers of other reagents are specified in the text.

Sample preparation for 2-D electrophoresis

Frozen mouse adipose tissue was ground in liquid nitrogen using a mortar and pestle. Frozen powders from individual blocks were thawed by adding 0.8 mL cold lysis buffer (7 M urea, 2 M thiourea, 4 % CHAPS, 40 mM Tris, and 60 mM DTT) and sonicated in an ice bath for ~1 min at 5 Watts (Sonic Dismembrator, Fisher Scientific). The sonicates were centrifuged at 14,000×*g* for 15 min at 4 °C. The supernatants were collected, and acetone was added to precipitated proteins, which were resolubilized using the above lysis buffer. The protein concentrations of the extracts were measured in triplicate using the BioRad Bradford-based protein assay with BSA as the standard.

2-D gel electrophoresis

For the separation of the first dimension, 40 g protein was diluted in 125 µL rehydration buffer and loaded onto an immobilized pH gradient (IPG) strip by passive in-gel rehydration overnight. The proteome was obtained with narrow range IPG strips (7 cm, pI4–7 and 6–10). The rehydration buffer contained 8 M urea, 2 % CHAPS, 0.2 % carrier ampholytes and 10 mM DTT for the linear pH 4–7 IPG strips. For the pH 6–10 IPG strips, rehydration was accomplished using 15 mg/mL Destreak reagent. Isoelectric focusing (IEF) was performed at 20 °C with a MultiPhor II system (Amersham Biosciences Corp. Piscataway, NJ) using a total of 12,000 V h with a maximum of 5,000 V.

For the separation of the second dimension, the IPG strips were removed from the MultiPhor II chamber and soaked for 15 min in 10 mL equilibration buffer for reduction [6 M urea, 30 % glycerol, 2 % SDS, 1 % DTT, and 0.05 M Tris (pH 8.8)] and then for 15 min in 10 mL equilibration buffer for alkylation (with 2.5 % iodoacetamide substituted for 1 % DTT). The strips were positioned on 10–14 % gradient SDS polyacrylamide gels in a BioRad Mini-PROTEAN 3 System at 160 V for 45 min. The gels were then fixed twice, each time for 30 min using 50 % methanol/7 % acetic acid. The protein spots were revealed by staining with either SYPRO-Ruby or SimplyBlue SafeStain.

Image analysis of the 2-D gels

Fluorescence images of the gels were captured with a FLA-5000 Fluor Imager (Fuji Photo Film Co, Ltd., Tokyo, Japan). Image analysis was performed with PDQuest software (version 8.0). One experimental set was created for the pI4–7 gels and another was created for the pI6–10 gels, with each set containing images of six gels (3 from SSAT-ko mice, 3 from SSAT-tg mice and 3 from wild type C57BL/6J mice). After automatic detection of the spots using PDQuest software, the spots were manually identified. The software provided individual spot “volumes” by density/area integration. To eliminate gel-to-gel variation, the individual spot volumes for each gel were normalized to the total spot volume for that gel. The normalized spot volume data from each experimental set were exported to Microsoft Excel, where the differentially expressed spots among the SSAT-ko mice, SSAT-tg mice and wild-type mice were tested for statistical significance using Student’s *t* tests ($P < 0.05$).

In-gel trypsin digestion

Differentially expressed spots were manually excised and diced into pieces of approximately 1 × 1 mm. Destaining of the excised gel pieces was performed by two 30-min washes with

50 % acetonitrile containing 50 mM ammonium bicarbonate. The proteins in the gel pieces were reduced with 50 mM ammonium bicarbonate buffer containing 1 % DTT for 30 min at 37 °C and then alkylated with 50 mM ammonium bicarbonate buffer containing 2.5 % iodoacetamide for 30 min in the dark at room temperature. Following dehydration with pure acetonitrile, the gel pieces were covered with approximately 40 μ L of 12.5 μ g/ μ L sequencing-grade trypsin (Promega, Madison, WI) in 50 mM ammonium bicarbonate buffer. Digestion, peptide extraction, and sample cleanup and desalting using ZipTips were performed as previously described (Duan et al 2008).

MALDI-TOF-TOF analysis

The desalted peptides from each spot were mixed 1:1 with matrix solution (1 % α -cyano-4-hydroxy cinnamic acid in 50 % acetonitrile and 0.1 % trifluoroacetic acid), and 1.0 μ L of each sample was applied to wells of an AnchorChip sample target plate and analyzed using a Bruker AutoFlex MALDI-TOF-TOF instrument. Peptide mass fingerprints were obtained using the reflective and positive ion mode. Mass spectra were collected from the sum of 100–400 laser shots, and mono-isotopic peaks were generated by FlexAnalysis software with a signal-to-noise ratio of 2:1. Mass peak value calculations were set to use two trypsin auto-digestion peptides with M+H values of 842.509 and 2,211.104 as internal standards. Proteins were identified by matching their calibrated peptide mass values to either the Swiss-Prot or NCBI nr protein databases for *Mus musculus* using an in-house version of Mascot Server 2.1 imbedded in Bruker Biotools software. The allowed match variances were a mass tolerance of 50 ppm, one missed trypsin cleavage, fixed modification of carbamidomethyl cysteine, and variable modification of methionine oxidation. For the samples that did not produce a “hit” with a confident score, peptide peaks with good signals were further fragmented using “laser-induced decomposition” to obtain LIFT-TOF/TOF spectra, and these MS/MS data alone or combined with the previously produced MS data were used to search against the protein database through the Mascot Server.

GeLC-MS analysis

The proteomic analysis of fat tissue from adipose-specific SAT1 knockout (FSAT1KO) mice was performed by gel electrophoresis–liquid chromatography–mass spectroscopy (GeLC-MS) using a Bruker HCTultra ion trap mass spectrometer as previously described (Duan et al. 2008, 2010).

Subcellular fractionation of adipose tissue

Mouse adipose tissues were ground into a powder in the presence of liquid nitrogen and resuspended into harvest buffer [10 mM HEPES (pH 7.9), 50 mM NaCl, 500 mM sucrose, 0.1 mM EDTA, 0.5 % Triton X-100, 1 mM DTT, 1 mM PMSF, 1 \times protease inhibitor cocktail]. After a 10-min incubation on ice, the lysates were then centrifuged at 1,000 rpm for 10 min at 4 °C to pellet the nuclei. The resulting supernatants were centrifuged at 14,000 \times g for 15 min at 4 °C to separate the membranes (pellets) and oil (upper layer of the supernatant) from the cytoplasmic fraction (major layer of the supernatant). The pellets containing the nuclei were washed in Buffer A [10 mM HEPES (pH 7.9), 10 mM KCl, 0.1 mM EDTA, 1 mM DTT, 1 mM PMSF, 1 \times protease inhibitor cocktail], and the nuclear

fractions were extracted in Buffer C [10 mM HEPES (pH 7.9), 500 mM NaCl, 0.1 mM EDTA, 0.1 % NP40, 1 mM DTT, 1 mM PMSF, 1× protease inhibitor cocktail].

Western blot analysis

Protein samples (30 g) from mouse adipose tissue homogenates or subcellular fractions were separated in a 10 % SDS polyacrylamide gel under reducing conditions and then transferred to a nitrocellulose membrane using a semidry blotting chamber (Bio-Rad, Hercules, CA) at 10 V for 30 min. The membrane was blocked with 5 % non-fat powdered milk in Tris-buffered saline (pH 7.6) containing 0.05 % Tween-20 (TBS/T) for 1 h at room temperature and then probed overnight at 4 °C with the indicated primary antibody, which was diluted 1:1,000 in blocking solution. After extensive washing, the membrane was incubated with the appropriate HRP-conjugated goat anti-mouse or mouse anti-rabbit secondary antibody at room temperature for 1 h. A Western Lightning Chemiluminescence Plus kit (PerkinElmer) was used according to the manufacturer's instructions, and the signals were captured using X-ray film.

Flux studies

Primary fat cell cultures were prepared from 22-week-old SSAT-ko, SSAT-wt and SSAT-tg mice as described previously (Bidaud et al. 2006; Blackburn 1995; Kajita et al. 2008; Klaunig et al. 1982). The cells were maintained in culture for at least 48 h for stabilization prior to their use in flux studies. Glucose (25 mM), which was uniformly labeled with ^{13}C (Cambridge Isotope Labs), was added to the cell cultures ($n = 5$) and incubated for 0, 1, 2 or 3 h. The glucose concentrations and incubation periods were chosen based on previously reported studies (Kharroubi et al. 1992). At the end of the incubation period, the metabolic processes were stopped by the addition of cold harvest buffer, and the cells were homogenized immediately. The nuclear, cytoplasmic, mitochondrial and microsomal fractions were separated using differential centrifugation methods (Cox and Emili 2006). We used the isotopomer spectral analysis (ISA) to determine the amount of acetyl-Spd and malonyl-CoA that was synthesized from ^{13}C -enriched glucose. The ISA model estimates the values for the two parameters controlling the flux of ^{13}C to the sampled acetyl-Spd and malonyl-CoA. D is the fractional contribution of the ^{13}C -labeled precursor to acetyl-CoA, and g (time) is the fractional amount of newly synthesized acetyl-Spd and malonyl-CoA in the sample. The fluxes in moles per time were estimated using the time course of change in g (time) as previously described (Bederman et al. 2004; Yoo et al. 2004). The model used here assumes that the flux of the precursors to the acetyl-CoA pools is constant during the time course of ^{13}C incubation. ISA uses equations for the probability of the appearance of each isotopomer based on test values for D and g (time). These probabilities are compared with the fractional abundance determined for each malonyl-CoA and acetyl-Spd isotopomer to obtain the best-fit solution (Kharroubi et al. 1992; Wong et al. 2004). The isotopomers of acetyl-CoA, acetylspermidine and malonyl-CoA were extracted from the primary cells as previously described (Kee et al. 2004) and subjected to mass spectrometry analysis to observe the fate of the ^{13}C atoms. Metabolites were identified and the ratio of ^{13}C to ^{12}C content (enrichment) was quantitated using a Bruker HCT Ultra LC/MS/MS coupled to a nanoLC pump system from Agilent. The ion source was maintained at 500 °C under nitrogen nebulization at a pressure of 70 psi. The heater gas (nitrogen) was at a pressure of

70 psi, the curtain gas pressure was at 35 psi, and the collision-activated dissociation gas pressure was held at high. The following parameters were set: turbo ion spray voltage of 4,500 V, declustering potential of 25 V, entrance potential of 10 V, collision energy of 5 V for enhanced mass spectra scans, collision cell exit potential of 11 V, and channel electron multiplier of 2,400 V. The samples were measured in electrospray negative and positive mode in a scan range of 50–900 m/z. Data analysis was performed using Metabolite Tools 1.1 software that was specifically designed for the prediction and rapid detection of metabolites. Mathematical modeling using ISA-based equations were used to calculate the acetylated polyamine and malonyl-CoA enrichment as previously described (Kelleher and Masterson 1992). Although acetyl-CoA participates in a wide range of metabolic pathways, polyamine and fat metabolism pathways are relatively simple, involve a limited number of reactions and are fed from limited precursor pools. Consequently, the flux analysis was less complex in this case than for large and extensively branched pathways. Because our data included concentrations of both labeled and unlabeled metabolites for each time point, simple graphic displays for the individual metabolites, which plot total metabolite concentration vs. time as well as the ratio of labeled to unlabeled metabolite vs. time, will reveal the key qualitative differences in flux in the SSAT-ko/tg vs. wild-type animals.

Crossbreeding of floxed SSAT-CKO mice and aP2-Cre mice

C57BL/6J mice and transgenic mice expressing Cre recombinase under control of the mouse aP2 promoter (aP2-Cre mice) were purchased from the Jackson Laboratory (He et al. 2003). A transgenic construct containing the Cre coding sequence under the control of the 5.4-kb Fabp4 (fatty acid-binding protein 4, adipocyte) promoter was introduced into unknown outbred donor eggs. The resulting male transgenic mice were crossed with B6.129-Ppargtm2Rev/J mice and subsequently crossed with C57BL/6J mice for 9 generations and were maintained with a C57BL/6J background. Cre recombinase expression was detected in the brown and white adipose tissue of these mice, whereas no expression was detected in the skeletal muscle. When crossed with a strain containing a loxP site-flanked sequence of interest, Cre-mediated recombination resulted in the deletion of the targeted gene specifically in the adipose tissue. This strain represents an effective tool for generating tissue-specific targeted mutants.

C57BL/6J mice containing the floxed SAT1 allele were maintained as previously described (Zahedi et al. 2012). These female mice were bred with aP2-Cre male mice to generate fat tissue-specific SSAT knockout mice (aP2-Cre⁺/SAT1^{lox/lox}), hereafter referred to as FSAT1KO mice. Upon breeding with Cre transgenic mice, portions of the 5' UTR, the entire region of exons 1–3 and portions of intron 3 of the SSAT gene were excised. The presence or absence of the floxed SSAT allele (located on the X chromosome) was determined by PCR using two primers (20 pmol each): forward primer (5' - GCTTCCTGAGTTTGCTTTTCTCG-3') and reverse primer (5' - CTCGTGACACCCATGGCCAAACC-3'). Mouse tail DNA was extracted and 1 µg was used for genotyping. PCR samples containing a final concentration of 1× Master Buffer, 1× reaction buffer, 2.5 mM MgCl₂, 0.2 mM dNTPs, and 1 U *Taq* polymerase enzyme were prepared. The reaction mixtures were cycled once at 95 °C for 1 min and 35 times at 94 °C for 30 s, 58 °C for 1 min, and 72 °C for 4 min, followed by a final extension of 72 °C for 10

min. The products were resolved with ethidium bromide using 2 % acrylamide gel electrophoresis in 1× TAE buffer to determine the presence of the SSAT-wt allele (206 bp) or the floxed SSAT allele (385 bp). Cre mice were genotyped according to instructions from the Jackson Laboratory (He et al. 2003). To detect tissue-specific recombination, instead of using the reverse primer for detecting floxed SSAT mice, a new reverse primer (5′-CTGATCTACTGTGTTTTAAGTGTG-3′) was used to assess the recombination of the SSAT gene.

All mice were fed standard chow diets containing 6 % fat ad libitum and had free access to water. The mice were housed in facilities providing a 12 h/12 h light/dark cycle. The animals were killed either by CO₂ asphyxiation or cervical dislocation. All subsequent procedures performed with these animals were in accordance with protocols approved by the Institute Animal Care and Use Committee (IACUC) and were conducted in accordance with the NIH Guide for the Care and Use of Laboratory Animals.

High-fat diet

The synthetic high-fat diet used for the diet-induced obesity model comprised 60 % calories from fat, 20 % calories from carbohydrates, and 20 % calories from protein (5.2 kcal/g) (Research Diets, Inc., New Brunswick, NJ). Control animals were fed a diet of standard rodent chow comprising 14 % calories from fat, 60 % calories from carbohydrates and 26 % calories from protein (4.1 kcal/g) (Prolab RMH 3100, PMI Nutrition International, Inc., Brentwood, MO). FSAT1KO mice and their WT littermates began consumption of the high-fat diet immediately post-weaning at 4 weeks of age and were monitored weekly for weight gain up to 27 weeks of age.

Glucose tolerance test (GTT)

Mice were fasted for 6 h by placing them in a clean cage without food. Mice were weighed, and a fasting glucose level was obtained from the venous blood via a small tail clip. Glucose (1 mg/g) was injected intraperitoneally, and blood glucose values were obtained after 0, 5, 15, 30, 60, 90 and 120 min.

Measurement of acetyl-CoA and malonyl-CoA by HPCE

The separation and quantitation of acetyl-CoA and malonyl-CoA in biological samples were performed based on the high performance capillary electrophoresis (HPCE) assay as previously described (Jell et al. 2007; Kee et al. 2004).

Histological study

Liver tissues, which were frozen in Tissue-Tek OCT (Sakura Finetek), were cut in 5- to 8- μ m-thick sections and mounted on glass slides. The slides were stained with hematoxylin and eosin (H&E) or Oil Red O to evaluate the fatty liver. For H&E staining, the frozen sections were air dried for 3 min to remove moisture, stained with filtered 0.1 % Mayer's hematoxylin for 10 min, rinsed in running ddH₂O for 5 min, and successively dipped in 0.5 % eosin 10 times, distilled H₂O 5 times, 50 % EtOH 10 times, and 70 % EtOH 10 times. The sections were then equilibrated in 95 % EtOH for 30 s and 100 % EtOH for 1 min, dipped in xylene several times, and air dried for several minutes. Finally, the slides were

mounted with Cytoseal XYL. For Oil Red O staining, the sections were air dried for 3 min, and placed in propylene glycol for 5 min to remove any water. They were then stained in pre-warmed Oil Red O solution for 10 min, placed in 85 % propylene glycol for 5 min, rinsed in two changes of distilled water, stained in Mayer's hematoxylin for 30 s, rinsed in running ddH₂O for 3 min, and finally mounted with glycerin jelly.

Statistical analysis

Data are expressed as mean values \pm standard error of the mean (SEM). Statistical comparisons were performed using unpaired, two-tailed Student's *t* tests. Differences were considered significant when $P < 0.05$.

Results

Measurement of acetyl-CoA flux in primary cultured adipocytes

In order to determine the extent of acetyl-CoA consumption that occurs through the polyamine pathway and fatty acid metabolic pathway, we evaluated the flux of carbon sources to acetyl-spermidine (acetyl-Spd) and malonyl-CoA by ISA, a stable isotope method for estimating the fractional contribution and the fractional new synthesis of carbon sources (Antoniewicz et al. 2007a, b). Figure 1a, b represents the distribution of the mass isotopomers of acetyl-Spd and malonyl-CoA across the three SSAT genotypes, ordered according to a gradient of increased expression of enzyme activity (i.e. SSAT-ko, SSAT-wt and SSAT-tg). ISA (*D*) value calculations using ISA model equations and Metran software (Kharroubi et al. 1992; Wong et al. 2004) indicated that glucose from the adipose tissue of SSAT-ko, SSAT-wt and SSAT-tg mice provided 15, 32 and 49 % of the acetyl-CoA for acetyl-Spd and malonyl-CoA, respectively. We also used the ISA model to determine the *g* (6 h), and these results indicated that 1, 16 and 90 % of the acetyl-Spd was synthesized de novo across the genotype gradient. Interestingly, de novo malonyl-CoA synthesis was 66, 61 and 22 % in these same mice indicating the shifting of acetyl-CoA towards fat metabolism. Finally, the acetyl-Spd and malonyl-CoA net fluxes were calculated by fitting the distribution of the mass isotopomers of acetyl-Spd, malonyl-CoA and acetyl-CoA to the metabolic network model (Antoniewicz et al. 2007a). Consistent with our hypothesis, overexpression of SSAT caused a 5.6-fold increase in flux towards polyamine acetylation and a 2.77-fold decrease in flux towards fatty acid synthesis. In contrast, SSAT knockout resulted in a 16.4-fold decrease in the acetyl-Spd flux and a 1.4-fold increase in the malonyl-CoA flux (Fig. 1c).

Proteomics study of WAT of SSAT-ko, SSAT-wt and SSAT-tg mice

Proteomic analysis was performed to analyze the global protein expression of WAT samples from SSAT-ko, SSAT-wt and SSAT-tg mice. The proteomic maps of WAT from the different mouse genotypes are shown in Fig. 2a. Comparing the SSAT-ko with SSAT-wt mice, we found 103 spots with significant differences in expression (full list of the proteins is shown in Supplementary Table 1). These differentially expressed spots represented 77 unique proteins. Of these 77 proteins, 26 proteins were present in multiple spots as a result of either multiple isoforms or post-translational modifications. Of the differentially expressed proteins, 22 were upregulated, 47 were downregulated and 8 were unique to the SSAT-ko

mice. A comparison of the SSAT-tg with SSAT-wt samples produced 24 upregulated spots, 21 downregulated spots and 4 unique spots to the SSAT-tg mice. The differentially expressed proteins from both comparisons were grouped into the following categories: lipogenesis (5 proteins), lipolysis/ β -oxidation (8 proteins), oxidative phosphorylation (7 proteins), amino acid metabolism (3 proteins), glucose metabolism (16 proteins), signal transduction (7 proteins), ER stress (4 proteins), antioxidants/cell stress response (12 proteins), structural (6 proteins) and miscellaneous (12 proteins). Of particular interest, 15 proteins exhibited 3-tier progression across the SSAT expression gradient Table 1. These proteins were repressed in the SSAT-ko mice and elevated in the SSAT-tg mice. The expression levels of six of these proteins are represented in 3-D view (Fig. 2b).

Because both the acetyl-CoA flux and the proteomics data showed an impact of SSAT on TCA cycle enzymes, we validated our results by Western blotting. Aliquots of samples from a separate group of SSAT-ko, SSAT-wt, and SSAT-tg animals ($n = 3$ each) were also analyzed by Western blotting with commercially available antibodies against aconitase, malate dehydrogenase and pyruvate dehydrogenase (Fig. 2b). Consistent with the aforementioned results, the expression levels of these 3 TCA cycle enzymes were reduced in the SSAT-ko mice compared to the SSAT-wt mice. However, only pyruvate dehydrogenase was found to be elevated in the SSAT-tg mice compared with the SSAT-wt mice (Fig. 2c).

Generation of SAT fat-specific knockout and its role in modulating the acetyl-CoA content

To determine how tissue-specific changes in SSAT expression will impact fat accumulation and the precise role of SSAT expression status in fat homeostasis and obesity, we generated adipose-specific SAT1 knockout (FSAT1KO) mice using the Cre-Lox method (Fig. 3a) and determined the acetyl-CoA content in the WAT and liver by high performance capillary electrophoresis (HPCE). Consistent with previous finding, the WAT acetyl-CoA level was ~32 % higher in the lysates from FSAT1KO mice than from the WT mice ($P < 0.05$) (Fig. 3b). As expected, there was no statistical difference in their acetyl-CoA pools of liver lysates (Fig. 3b) suggesting that the specific depletion of SSAT in adipose tissue does not interfere with the flux in liver tissue.

The WATs of FSAT1KO and SSAT-ko mice show similar proteomic patterns

WAT samples from SSAT-wt and FSAT1KO mice were analyzed using GeLC-MS method to obtain the following proteomics data. Twenty-nine proteins were found to be downregulated in the FSAT1KO mice and 30 proteins were found to be upregulated in the FSAT1KO mice compared to the SSAT-wt mice (Supplementary Table 2). Thirteen of these proteins were consistent with the proteomics data obtained in the whole-body samples from the SSAT-ko vs SSAT-wt mice (Table 2), including 9 proteins that were downregulated in response to the depletion of the SSAT enzyme [acyl-CoA binding protein (ACBP), α -enolase, carbonic anhydrase 3, cytochrome *c*, fructose-bisphosphate aldolase, glutathione *S*-transferase pi, superoxide dismutase (Cu-Zn), tubulin and vimentin] and 4 proteins that were upregulated in response to the depletion of SSAT (adipocyte lipid-binding protein, heat shock 70 kDa protein, L-lactate dehydrogenase, and fatty acid-binding protein).

Ablation of SSAT in WAT promotes mouse growth and lipid storage

We have previously shown that whole-body knockout of SSAT has been previously shown to facilitate fat accumulation on a high-fat diet (Jell et al. 2007). It is of interest to determine whether this is due to a systemic metabolic response or to local changes in the WAT. To first analyze the effect of SSAT on adipose tissue, body weight gain was monitored weekly for wild-type control littermates and FSAT1KO mice ($n = 6$ mice per group) over 23 weeks between the ages of 4 and 27 weeks (Fig. 3c). Immediately before they were challenged with a high-fat diet (HFD) at 4 weeks of age, their initial body weights were similar (18.33 ± 0.52 g for SSAT-wt vs. 18.83 ± 1.33 g for FSAT1KO). Changes in the body growth of the FSAT1KO mice were observable from as early as 18 weeks of age. At 27 weeks of age, the average body weights were 45.13 ± 2.23 g for the SSAT-wt mice and 52.28 ± 1.62 g for the FSAT1KO mice. The FSAT1KO mice weighed approximately 15 % more than the SSAT-wt mice.

To determine the cause of the increased body weight of the FSAT1KO mice, individual organs were harvested and weighed (Fig. 3d). The FSAT1KO and control mice displayed no significant differences in the weights of their lean organs, such as the heart, kidney, brain and thigh muscle. The average weight of heart from both groups of mice was the same (249.8 mg for SSAT-wt vs. 251.3 mg for FSAT1KO). Notably, the livers of the FSAT1KO mice were significantly heavier than those of the SSAT-wt mice. The FSAT1KO mice exhibited a ~40 % increase in their liver weight which accounted for 43 % of the weight gain. We next examined histological sections of the liver, a secondary fat storage organ. Liver tissue sections from 3 SSAT-wt mice and 3 FSAT1KO mice were stained with H&E or Oil Red O to evaluate the fatty liver. Note that both groups of mice had overloaded lipid droplets and developed fatty livers, as revealed by Oil Red O staining (Fig. 3e) after 23 weeks of HFD consumption. The livers of the SSAT-wt littermates were histologically normal. The livers of the FSAT1KO mice showed disruption of normal liver architecture, as indicated by H&E staining (Fig. 3e). Oil Red O staining of the liver sections from the FSAT1KO mice on a HFD showed particularly enlarged lipid droplets and a marked increase in lipid deposition compared to the controls, which is indicative of advanced steatosis.

Ablation of SSAT in WAT affects glucose homeostasis in mice

To assess the effects of SSAT deficiency in WAT on glucose homeostasis in intact mice, we performed a glucose tolerance test using intraperitoneally injected glucose to determine the ability of the mice to clear glucose from their blood (Fig. 3f). Upon the IP injection of glucose, both groups of SSAT-wt and FSAT1KO mice on HFDs showed the same level of fasting glucose (210 mg/dL), which was much higher than normal wild-type C57BL/6J mice (120 mg/dL), and HFD-fed FSAT1KO and SSAT-wt mice both exhibited reduced rates of glucose clearance, indicating that 23 weeks of HFD consumption gives rise to a diabetes-like condition in mice. However, the glucose clearance rate for the SSAT-wt mice was slightly better than seen in the FSAT1KO mice.

Activation of the AMPK pathway in adipose tissue is affected by SSAT expression

The expression and phosphorylation of the catalytic α subunit of AMPK, the regulatory β subunits of AMPK and their downstream enzyme acetyl-CoA carboxylase (ACC) were

evaluated by Western blotting. Eight samples from each of the SSAT-ko, SSAT-wt and SSAT-tg groups were used for this analysis, and three samples are shown representatively in Fig. 4a. β -Actin was used as an internal control. In comparison with the SSAT-wt mice, the expression level and phosphorylation of AMPK α were increased fivefold and 1.9-fold, respectively, in the SSAT-tg mice. There was no visible change in the expression level of the regulatory β 1/2 subunits of AMPK; nevertheless, phosphorylation of the β 1 subunit was 5.3 times higher in the SSAT-tg mice compared to the SSAT-wt mice. The phosphorylation of these AMPK subunits in the SSAT-ko mice were unchanged compared to the SSAT-wt mice. We also evaluated the protein level and phosphorylation state of the catalytic α subunit of AMPK in WAT and liver tissue from SSAT-wt and FSAT1KO mice by Western blotting analysis (Fig. 4b). Six samples from each group were used for this analysis, and β -actin was used as an internal control. In comparison with the SSAT-wt mice, the phosphorylation of AMPK α was decreased in the WAT of the FSAT1KO mice by ~50 %, which is consistent with the results from the SSAT-ko mice.

No difference in the levels of AMPK and pAMPK α was observed in the liver tissues from the FSAT1KO and SSAT-wt mice. This result suggests that although the histological data showed increased lipid deposition in liver tissues of the FSAT1KO mice, the hepatic AMPK pathway was not perturbed in order to reduce the SSAT level in the adipose tissue.

Discussion

Sustained and deregulated overexpression of SSAT, such as in SSAT-tg mice, results in the loss of polyamines, which releases the negative feedback control of anabolic enzymes, leading to increased synthesis; the net-result is heightened polyamine turnover, a massive increase in metabolic flux through the pathway with little change in polyamine content. Under these conditions, there would be a markedly increased utilization of polyamine precursors such as acetyl-CoA (Kramer et al. 2008) to the point that their pools may be wholly or partially depleted. Acetyl-CoA has a fundamental role in WAT substrate partitioning, and its cellular abundance is important for the malonyl-CoA-mediated effects on lipid oxidation and lipogenesis as well as in polyamine acetylation. Our flux data show that increased SSAT activity increases acetyl-CoA consumption for polyamine acetylation and reduces the availability of acetyl-CoA for fat synthesis. More importantly, our data show that under physiological conditions, in which most SSAT expression is repressed at the translational level (Perez-Leal et al. 2012; Perez-Leal and Merali 2012), 61 % of the acetyl-CoA is partitioned towards fatty acid synthesis and that the 4 % increase in this partition over several weeks as seen in the SSAT-ko mice is likely to contribute to the obese phenotype.

A previous proteomics study on the liver tissues of SSAT-tg mice revealed 23 proteins that are associated with the activation of polyamine catabolism (Cerrada-Gimenez et al. 2010). Another study on SSAT-tg mice showed increased levels of PGC-1, along with a high basal metabolic rate, improved glucose tolerance, high insulin sensitivity, and enhanced expression of the oxidative phosphorylation (OXPHOS) genes in WAT (Pirinen et al. 2007). Particularly when cells undergo differentiation, there appears to be a specific and required induction in the spermidine pools (Bethell and Pegg 1981; Erwin et al. 1984; Vuohelainen et

al. 2010), indicating that impaired adipogenesis is one of the possible reasons for the lean phenotype of SSAT-tg mice, in which spermidine is depleted due to the acetylation caused by the induction of SSAT activity. Collectively, these studies indicate an evident linkage between polyamine homeostasis and energy metabolism in fat tissue, and perturbations in polyamine metabolism may contribute to the development of obesity.

We studied the proteomes in the WAT of SSAT-ko, SSAT-wt and SSAT-tg mice to understand how these metabolic changes occur on a global scale. The results of our evaluation of this SSAT expression gradient in mice are self-validating. Proteomics indicated that lipogenesis was increased and lipolysis and β -oxidation were decreased in SSAT-ko mice, in agreement with the fact that SSAT-ko mice tended to develop obesity. Two enzymes involved in lipogenesis were markedly increased (more than fourfold) in the SSAT-ko mice. Glycerol-3-phosphate dehydrogenase provides the glycerol-3-phosphate (G3P) needed for the triglyceride backbone in adipocytes. Adipocyte fatty acid-binding protein (AFABP) is a serum biomarker that is closely related to obesity and metabolic syndrome (Xu et al. 2006). Proteins involved in lipolysis showed low expression levels in the SSAT-ko mice. Several forms of carbonic anhydrase were all decreased in these mice. Carbonic anhydrase 3 is the most abundant protein in adipose tissue, and a previous study indicated its reduction in obesity and its possible role in leptin secretion (Alver et al. 2004). Two enzymes involved in the β -oxidation pathway, a major source of ATP and acetyl-CoA, were decreased in the SSAT-ko mice, including enoyl-CoA hydratase and hydroxylacyl-coenzyme A dehydrogenase. Our proteomic analysis also found a large number of enzymes responsible for glucose metabolism that were suppressed in the SSAT-ko mice and elevated in the SSAT-tg mice as compared to the SSAT-wt mice.

Several OXPHOS components of the mitochondrial respiratory chain were significantly increased in the WAT of the SSAT-tg mice and were present at relatively low levels in the SSAT-ko mice, including cytochrome b5, ubiquinol-cytochrome-*c* reductase complex core protein 1, electron transfer flavoprotein (beta-subunit) and ATP synthase. These enzymes are of pivotal importance in almost all organisms and are especially valuable in SSAT-tg mice, in which ATP is deficient due to the enhanced polyamine flux (Pirinen et al. 2007).

We hypothesized that the tissue-specific absence of SSAT activity in the adipose tissue drives the obese phenotype of SSAT-ko mice. This hypothesis is supported by our observation that the WAT, but not liver or muscle, of the SSAT-ko mice has increased acetyl-CoA and malonyl-CoA levels (Jell et al. 2007). FSAT1KO mice, which have a specific depletion of SSAT activity in adipose tissue, allowed for a critical test of this hypothesis. We found that HFD-fed FSAT1KO mice readily gained more weight after 18 weeks of age and weighed ~15 % more than the SSAT-wt mice at 27 weeks. Furthermore, the livers of the FSAT1KO mice weighed ~40 % more than those of the SSAT-wt mice. Our histology study showed particularly enlarged lipid droplets in FSAT1KO liver tissue sections, suggesting that the adipose tissue-specific depletion of SSAT also has an impact on the liver.

The proteome of the WAT from the FSAT1KO mice showed high similarity to that from the SSAT-ko mice. Enzymes involved in lipolysis/lipogenesis, including acyl-CoA binding protein (ACBP), carbonic anhydrase 3, adipocyte lipid-binding protein, fatty acid-binding

protein; enzymes involved in glycolysis, including α -enolase, fructose-bisphosphate aldolase, L-lactate dehydrogenase, glutathione *S*-transferase pi; and OXPHOS enzymes, including cytochrome *c*, superoxide dismutase [Cu–Zn], showed similar expression patterns as those in SSAT-ko mice.

AMPK plays a central role in cellular energy homeostasis (Miranda et al. 2007). The metabolic regulatory function of AMPK originates from its activation status upon changes in the AMP/ATP ratio during exercise or other cellular factors, including the presence of the hormones adiponectin (Yamauchi et al. 2002) and leptin (Minokoshi et al. 2002) or the administration of AICAR (Winder 2000). An elevated AMP/ATP ratio leads to the phosphorylation of AMPK on its catalytic α subunit and regulatory β and γ subunits and subsequently stimulates its kinase activity to phosphorylate/inhibit acetyl-CoA carboxylase (ACC), which catalyzes the carboxylation of acetyl-CoA to malonyl-CoA, a crucial step in the fatty acid synthesis pathway (Mao et al. 2009). A significant portion of AMPK function is mediated by its ability to modulate the levels of acetyl-CoA and malonyl-CoA. The overall effect of AMPK activation on fat metabolism is the inhibition of fatty acid synthesis and stimulation of β -oxidation. Polyamine flux, which is driven by polyamine acetylation and excretion in the urine, causes a significant depletion of the substrate acetyl-CoA and a loss of ATP, thus activating AMPK, which in turn inhibits the ability of ACC to convert acetyl-CoA into malonyl-CoA. When the levels of the substrate acetyl-CoA and the ACC activity were low, the amount of malonyl-CoA in the adipose tissue of the SSAT-tg mice was exceedingly low. The ACC knockout mouse model is comparatively similar to the SSAT-tg mouse model with respect to fat metabolism, as the ACC activity is decreased in both systems. ACC knockout mice with markedly reduced levels of malonyl-CoA show a ~50 % reduction in body fat compared to wild-type mice (Mao et al. 2009). In the SSAT-ko system, acetyl-CoA and ATP accumulate due to the decelerated polyamine flux; AMPK is not activated, thereby leading to less phosphorylation of ACC and triggering its activity to convert acetyl-CoA to malonyl-CoA; and elevated malonyl-CoA blocks CPT1, which transfers fatty acids into the mitochondria for β -oxidation. Our experiments on the FSAT1KO mice provided a better understanding of this mechanism. AMPK was activated to a lesser extent in the WAT of the FSAT1KO mice compared to the SSAT-wt mice, whereas different levels of AMPK activation were not found in the liver tissue, further suggesting that the expression status of SSAT has an effect on AMPK activation, which subsequently regulates energy metabolism.

In conclusion, our results demonstrate that the modification of the acetyl-CoA flux by genetic modulation of SSAT causes a combination of changes in WAT that involve lipolysis, energy metabolism and calorie loss resulting from polyamine export, thereby influencing the accumulation of body fat.

Supplementary Material

Refer to Web version on PubMed Central for supplementary material.

Abbreviations

SSAT	Spermidine/spermine <i>N</i> ¹ -acetyltransferase
AMPK	AMP-activated protein kinase
ACC	Acetyl-CoA carboxylase
CPT-1	Carnitine palmitoyltransferase-1

References

- Alver A, Keha EE, Ucar F, Ovali E. The effect of carbonic anhydrase inhibition on leptin secretion by rat adipose tissue. *J Enzyme Inhib Med Chem.* 2004; 19:181–184. [PubMed: 15449734]
- Antoniewicz MR, Kelleher JK, Stephanopoulos G. Elementary metabolite units (EMU): a novel framework for modeling isotopic distributions. *Metab Eng.* 2007a; 9:68–86. [PubMed: 17088092]
- Antoniewicz MR, Kraynie DF, Laffend LA, Gonzalez-Lergier J, Kelleher JK, Stephanopoulos G. Metabolic flux analysis in a nonstationary system: fed-batch fermentation of a high yielding strain of *E. coli* producing 1,3-propanediol. *Metab Eng.* 2007b; 9:277–292. [PubMed: 17400499]
- Bederman IR, Reszko AE, Kasumov T, David F, Wasserman DH, Kelleher JK, Brunengraber H. Zonation of labeling of lipogenic acetyl-CoA across the liver: implications for studies of lipogenesis by mass isotopomer analysis. *J Biol Chem.* 2004; 279:43207–43216. [PubMed: 15284242]
- Bethell DR, Pegg AE. Polyamines are needed for the differentiation of 3T3–L1 fibroblasts into adipose cells. *Biochem Biophys Res Commun.* 1981; 102:272–278. [PubMed: 6796085]
- Bidaud I, Monteil A, Nargeot J, Lory P. Properties and role of voltage-dependent calcium channels during mouse skeletal muscle differentiation. *J Muscle Res Cell Motil.* 2006; 27:75–81. [PubMed: 16538437]
- Blackburn G. Effect of degree of weight loss on health benefits. *Obes Res.* 1995; 3(Suppl 2):211s–216s. [PubMed: 8581779]
- Cerrada-Gimenez M, Hayrinen J, Juutinen S, Reponen T, Janne J, Alhonen L. Proteomic analysis of livers from a transgenic mouse line with activated polyamine catabolism. *Amino Acids.* 2010; 38:613–622. [PubMed: 20012117]
- Cox B, Emili A. Tissue subcellular fractionation and protein extraction for use in mass spectrometry-based proteomics. *Nat Protoc.* 2006; 1:1872–1878. [PubMed: 17487171]
- Duan X, Kelsen SG, Merali S. Proteomic analysis of oxidative stress-responsive proteins in human pneumocytes: insight into the regulation of DJ-1 expression. *J Proteome Res.* 2008; 7:4955–4961. [PubMed: 18817430]
- Duan X, Kelsen SG, Clarkson AB Jr, Ji R, Merali S. SILAC analysis of oxidative stress-mediated proteins in human pneumocytes: new role for treacle. *Proteomics.* 2010; 10:2165–2174. [PubMed: 20340163]
- Erwin BG, Bethell DR, Pegg AE. Role of polyamines in differentiation of 3T3–L1 fibroblasts into adipocytes. *Am J Physiol.* 1984; 246:C293–C300. [PubMed: 6422770]
- Fogel-Petrovic M, Vujcic S, Brown PJ, Haddox MK, Porter CW. Effects of polyamines, polyamine analogs, and inhibitors of protein synthesis on spermidine-spermine *N*¹-acetyltransferase gene expression. *Biochemistry.* 1996; 35:14436–14444. [PubMed: 8916930]
- He W, Barak Y, Hevener A, Olson P, Liao D, Le J, Nelson M, Ong E, Olefsky JM, Evans RM. Adipose-specific peroxisome proliferator-activated receptor gamma knockout causes insulin resistance in fat and liver but not in muscle. *Proc Natl Acad Sci USA.* 2003; 100:15712–15717. [PubMed: 14660788]
- Jell J, Merali S, Hensen ML, Mazurchuk R, Spornyak JA, Diegelman P, Kisiel ND, Barrero C, Deeb KK, Alhonen L, et al. Genetically altered expression of spermidine/spermine *N*¹-acetyltransferase affects fat metabolism in mice via acetyl-CoA. *J Biol Chem.* 2007; 282:8404–8413. [PubMed: 17189273]

- Kajita K, Mune T, Ikeda T, Matsumoto M, Uno Y, Sugiyama C, Matsubara K, Morita H, Takemura M, Seishima M, et al. Effect of fasting on PPAR γ and AMPK activity in adipocytes. *Diabetes Res Clin Pract.* 2008; 81(2):144–149. [PubMed: 18562038]
- Kee K, Foster BA, Merali S, Kramer DL, Hensen ML, Diegelman P, Kisiel N, Vujcic S, Mazurchuk RV, Porter CW. Activated polyamine catabolism depletes acetyl-CoA pools and suppresses prostate tumor growth in TRAMP mice. *J Biol Chem.* 2004; 279:40076–40083. [PubMed: 15252047]
- Kelleher JK, Masterson TM. Model equations for condensation biosynthesis using stable isotopes and radioisotopes. *Am J Physiol.* 1992; 262:E118–E125. [PubMed: 1733242]
- Kharroubi AT, Masterson TM, Aldaghlis TA, Kennedy KA, Kelleher JK. Isotopomer spectral analysis of triglyceride fatty acid synthesis in 3T3–L1 cells. *Am J Physiol.* 1992; 263:E667–E675. [PubMed: 1415685]
- Klaunig JE, Goldblatt PJ, Hinton DE, Lipsky MM, Knipe SM, Trump BF. Morphologic and functional studies of mouse hepatocytes in primary culture. *Anat Rec.* 1982; 204:231–243. [PubMed: 6130724]
- Kramer DL, Diegelman P, Jell J, Vujcic S, Merali S, Porter CW. Polyamine acetylation modulates polyamine metabolic flux, a prelude to broader metabolic consequences. *J Biol Chem.* 2008; 283:4241–4251. [PubMed: 18089555]
- Mao J, Yang T, Gu Z, Heird WC, Finegold MJ, Lee B, Wakil SJ. aP2-Cre-mediated inactivation of acetyl-CoA carboxylase 1 causes growth retardation and reduced lipid accumulation in adipose tissues. *Proc Natl Acad Sci USA.* 2009; 106:17576–17581. [PubMed: 19805143]
- McCloskey DE, Pegg AE. Properties of the spermidine/spermine N1-acetyltransferase mutant L156F that decreases cellular sensitivity to the polyamine analogue M1, N1-bis(ethyl)norspermine. *J Biol Chem.* 2003; 278:13881–13887. [PubMed: 12578836]
- Minokoshi Y, Kim YB, Peroni OD, Fryer LG, Muller C, Carling D, Kahn BB. Leptin stimulates fatty-acid oxidation by activating AMP-activated protein kinase. *Nature.* 2002; 415:339–343. [PubMed: 11797013]
- Miranda N, Tovar AR, Palacios B, Torres N. AMPK as a cellular energy sensor and its function in the organism. *Rev Invest Clin.* 2007; 59:458–469. [PubMed: 18402338]
- NCHS. NCHS dataline. *Public Health Rep.* 2008; 123:390–393.
- Pegg AE. Spermidine/spermine-N(1)-acetyltransferase: a key metabolic regulator. *Am J Physiol Endocrinol Metab.* 2008; 294:E995–E1010. [PubMed: 18349109]
- Pegg AE, McCann PP. Polyamine metabolism and function. *Am J Physiol.* 1982; 243:C212–C221. [PubMed: 6814260]
- Perez-Leal O, Merali S. Regulation of polyamine metabolism by translational control. *Amino Acids.* 2012; 42:611–617. [PubMed: 21811825]
- Perez-Leal O, Barrero CA, Clarkson AB, Casero RA Jr, Merali S. Polyamine-regulated translation of spermidine/spermine-N1-acetyltransferase. *Mol Cell Biol.* 2012; 32:1453–1467. [PubMed: 22354986]
- Pietila M, Alhonen L, Halmekyto M, Kanter P, Janne J, Porter CW. Activation of polyamine catabolism profoundly alters tissue polyamine pools and affects hair growth and female fertility in transgenic mice overexpressing spermidine/spermine N1-acetyltransferase. *J Biol Chem.* 1997; 272:18746–18751. [PubMed: 9228047]
- Pirinen E, Kuulasmaa T, Pietila M, Heikkinen S, Tusa M, Itkonen P, Boman S, Skommer J, Virkamaki A, Hohtola E, et al. Enhanced polyamine catabolism alters homeostatic control of white adipose tissue mass, energy expenditure, and glucose metabolism. *Mol Cell Biol.* 2007; 27:4953–4967. [PubMed: 17485446]
- Vuohelainen S, Pirinen E, Cerrada-Gimenez M, Keinänen TA, Uimari A, Pietila M, Khomutov AR, Janne J, Alhonen L. Spermidine is indispensable in differentiation of 3T3–L1 fibroblasts to adipocytes. *J Cell Mol Med.* 2010; 14:1683–1692. [PubMed: 19538475]
- Wang Y, Casero RA Jr. Mammalian polyamine catabolism: a therapeutic target, a pathological problem, or both? *J Biochem.* 2006; 139:17–25. [PubMed: 16428315]
- Winder WW. AMP-activated protein kinase: possible target for treatment of type 2 diabetes. *Diabetes Technol Ther.* 2000; 2:441–448. [PubMed: 11467346]

- Wong MS, Raab RM, Rigoutsos I, Stephanopoulos GN, Kelleher JK. Metabolic and transcriptional patterns accompanying glutamine depletion and repletion in mouse hepatoma cells: a model for physiological regulatory networks. *Physiol Genomics*. 2004; 16:247–255. [PubMed: 14612591]
- Xu A, Wang Y, Xu JY, Stejskal D, Tam S, Zhang J, Wat NM, Wong WK, Lam KS. Adipocyte fatty acid-binding protein is a plasma biomarker closely associated with obesity and metabolic syndrome. *Clin Chem*. 2006; 52:405–413. [PubMed: 16423904]
- Yamauchi T, Kamon J, Minokoshi Y, Ito Y, Waki H, Uchida S, Yamashita S, Noda M, Kita S, Ueki K, et al. Adiponectin stimulates glucose utilization and fatty-acid oxidation by activating AMP-activated protein kinase. *Nat Med*. 2002; 8:1288–1295. [PubMed: 12368907]
- Yoo H, Stephanopoulos G, Kelleher JK. Quantifying carbon sources for de novo lipogenesis in wild-type and IRS-1 knockout brown adipocytes. *J Lipid Res*. 2004; 45:1324–1332. [PubMed: 15102881]
- Zahedi K, Barone SL, Xu J, Steinbergs N, Schuster R, Lentsch AB, Amlal H, Wang J, Casero RA Jr, Soleimani M. Hepatocyte-specific ablation of spermine/spermidine-N1-acetyltransferase gene reduces the severity of CCl4-induced acute liver injury. *Am J Physiol Gastrointest Liver Physiol*. 2012; 303:G546–G560. [PubMed: 22723264]

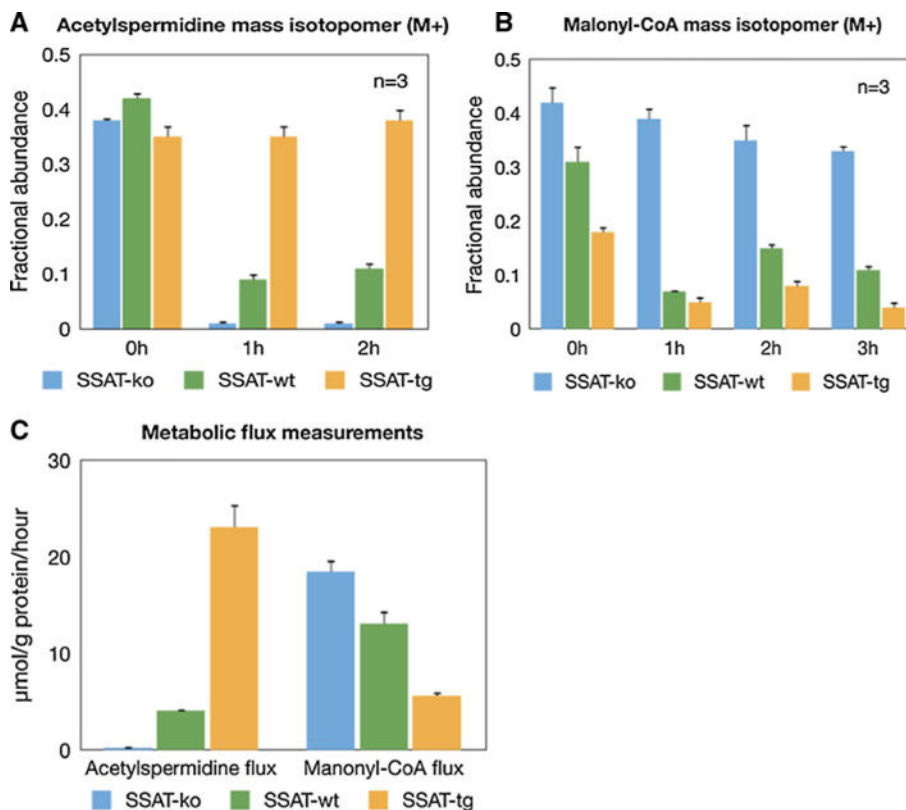


Fig. 1.
a The distribution of mass isotopomers of acetylspermidine (acetyl-Spd) across the three SSAT genotypes (SSAT-ko, SSAT-wt, and SSAT-tg). **b** The distribution of mass isotopomers of malonyl-CoA (acetyl-Spd) across the three SSAT genotypes (SSAT-ko, SSAT-wt, and SSAT-tg). **c** Metabolic flux measurement across the three SSAT genotypes (SSAT-ko, SSAT-wt, and SSAT-tg)

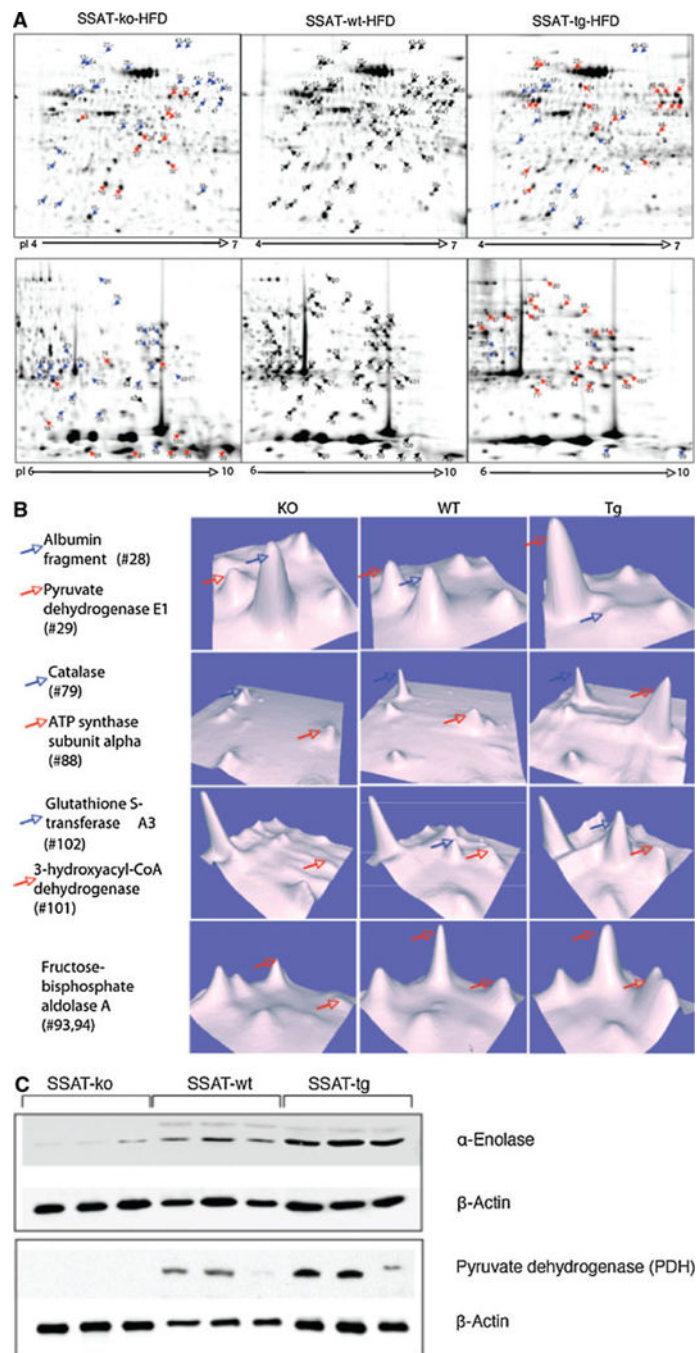


Fig. 2.
a SSAT-ko, SSAT-tg and wt adipose tissue proteome map of pH 4–7 (*top panel*) and pH 6–10 (*bottom panel*). The proteins were stained with SYPRO-Ruby and images compared by PD Quest software. The *numbers* correspond to the spot numbers in Supplementary Table 1. As compared to wt, *blue arrows* represent downregulation and *red arrows* represent upregulation. **b** Expression levels of representative proteins of Table 1. The 3D images were provided by PD Quest software. The height of peaks indicates the intensity of protein spots. **c** Protein abundance of α -enolase and pyruvate dehydrogenase (PDH) in mouse adipose

tissue, as determined by western blot. The level of β -actin was used for normalization (color figure online)

Author Manuscript

Author Manuscript

Author Manuscript

Author Manuscript

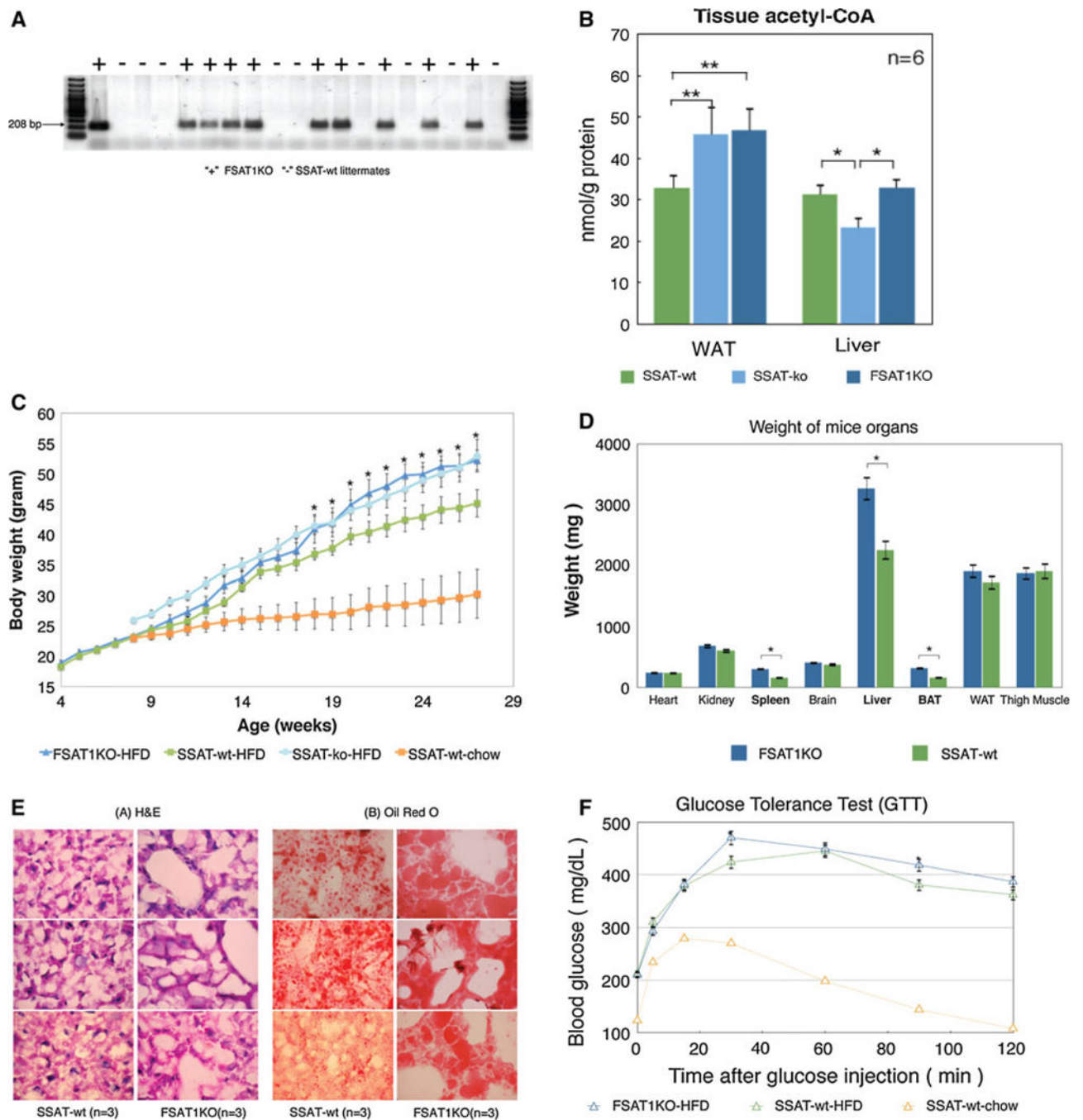


Fig. 3.
a Genotyping of floxed SSAT mice and FSAT1KO mice. The male pups from crossbreeding of floxed SSAT mice with aP2-Cre mice were screened for their tissue-specific recombination. The *right lane* indicates wild-type mice without specific knockout of SAT1 gene. The “+” indicates the fat-specific SAT1 knockout (FSAT1KO) mice. The “-” indicates the wild-type littermates. **b** Acetyl-CoA pools in WAT and liver lysates from SSAT-wt, SSAT-ko and FSAT1KO. **c** Growth curve of the mice during a high-fat diet. Body weight gain in wild-type control littermates (WT) and fat-specific SAT1 gene knockout (FSAT1KO)

mice ($n = 6$ mice per group). $*P < 0.05$; their initial body weights were similar: 18.33 ± 0.52 g (WT) versus 18.83 ± 1.33 g (FSAT1KO). **d** Organ weights of the mice. Wild-type control littermates (WT) and fat-specific SAT1 gene knockout (FSAT1KO) mice ($n = 6$ mice per group). $*P < 0.05$. The average weight of heart from both groups of mice was the same. The spleen, liver and brown fat tissue (BAT) from FSAT1KO were significantly heavier than WT. White adipose tissue (WAT) were abdominal fat pads from these mice. **e** Mice liver histology after 23-week high-fat diet. Liver from wild-type control littermates (WT) and fat-specific SAT1 gene knockout (FSAT1KO) mice were stained with hematoxylin and eosin (H&E), or Oil Red O to evaluate the fatty liver. Note that more lipid accumulation is present in the FSAT1KO mice compared to the control WT mice ($n = 3$ mice per group). **f** Glucose tolerance test (GTT). Mice were fasted for 6 h and evaluated for their glucose tolerance in an intraperitoneal glucose tolerance test (1 mg per gram of body weight). Blood glucose concentration was measured at 0, 5, 15, 30, 60, 90 and 120 min ($n = 6$ mice per group). FSAT1KO indicates fat tissue-specific SAT1 knockout mice on high-fat diet. *WT* wild-type mice on high-fat diet. *WT-chow* indicate wild-type mice on normal diet

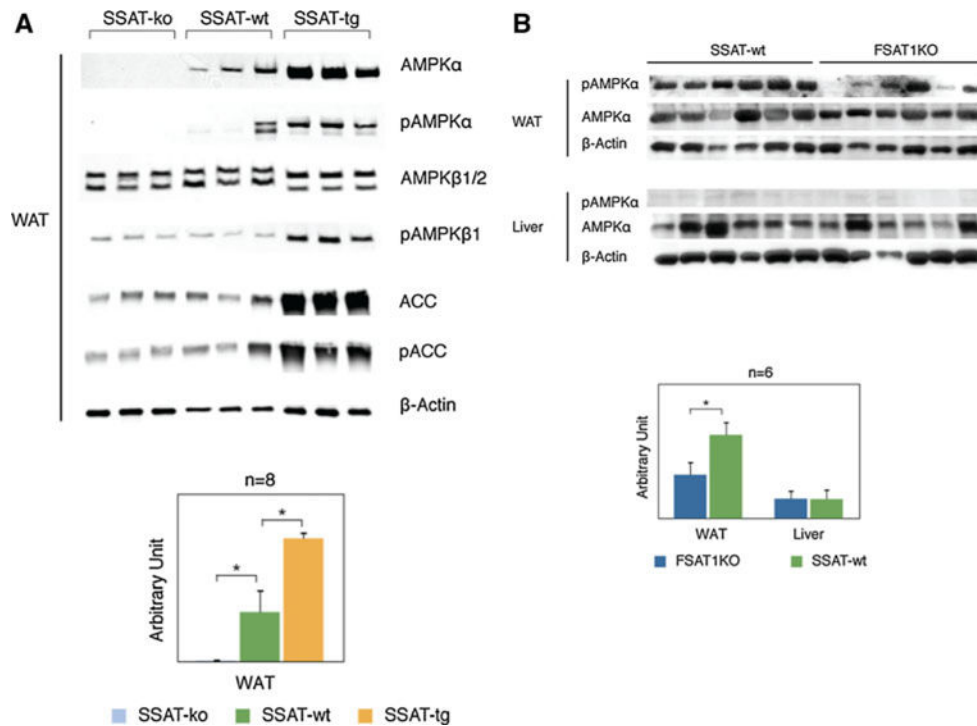


Fig. 4.
a *AMPK* phosphorylated AMPK α (pAMPK α), *AMPK β 1/2* phosphorylated AMPK β 1 (pAMPK β 1), *ACC* phosphorylated ACC (pACC) protein levels in adipose tissues from SSAT-ko, wt and SSAT-tg mice. Western blot results were detected with polyclonal antibodies (Cell Signaling Technology, Inc., Danvers, MA) against each protein. The *bottom panel* shows relative pAMPK α protein levels in adipose tissue after normalization with β -actin. Results are displayed as group means \pm SEM. * P < 0.05, *t* test was done between SSAT-ko with wt, or between SSAT-tg with wt. **b** AMPK α activation status in FSAT1KO WAT and liver tissues. Protein levels and phosphorylation state of AMPK α in WAT and liver from wild-type control littermates (WT) and FSAT1KO mice ($n = 6$, each) were evaluated by western blot analysis. β -Actin was used as internal control

Table 1

Proteomic trends based on proteins showing 3-tier progression across SSAT-ko, SSAT-wt, and SSAT-tg animals

Spot	Protein ID	Normalized 2D spot volume (n = 4)			P value (vs WT)	
		SSAT-KO	SSAT-WT	SSAT-tg	KO	tg
Lipolysis/ β -oxidation						
101	3-Hydroxyacyl-CoA dehydrogenase type-2	377 \pm 156	1,343 \pm 308	2,807 \pm 249	0.001	0.001
Oxidative phosphorylation						
88	ATP synthase subunit alpha, mitochondrial	432 \pm 404	1,227 \pm 361	3,798 \pm 1,173	0.041	0.006
90	Electron transfer flavoprotein subunit beta	1,997 \pm 490	2,731 \pm 327	3,988 \pm 581	0.047	0.009
Amino acid metabolism						
74	Delta-1-pyrroline-5-carboxylate dehydrogenase	<DL	298 \pm 133	1,028 \pm 557	0.004	0.043
Glucose metabolism						
29	Pyruvate dehydrogenase E1 component subunit beta	2,394 \pm 999	6,435 \pm 1,146	10,476 \pm 2,814	0.002	0.040
44	Malate dehydrogenase cytoplasmic	<DL	1,790 \pm 313	3,286 \pm 501	0.001	0.007
45	α -Enolase	1,589 \pm 279	2,341 \pm 214	5,270 \pm 1,360	0.005	0.021
46		1,246 \pm 537	1,393 \pm 590	7,029 \pm 2,078	0.725	0.004
47		4,688 \pm 902	8,143 \pm 1,798	10,865 \pm 1,446	0.014	0.017
75	NADP-dependent malic enzyme	<DL	1,517 \pm 320	3,624 \pm 1,462	<0.001	0.048
80	Aconitate hydratase, mitochondrial	146 \pm 169	643 \pm 118	1,275 \pm 407	0.003	0.025
93	Fructose-bisphosphate aldolase A	1,670 \pm 636	2,987 \pm 654	4,380 \pm 975	0.028	0.151
94		2,398 \pm 1,083	6,562 \pm 2,734	7,670 \pm 552	0.030	0.956
ER stress/UPR						
13	78 kDa glucose-regulated protein	570 \pm 151	1,563 \pm 251	1,851 \pm 314	0.001	0.028
14		827 \pm 474	2,661 \pm 393	3,378 \pm 299	0.001	0.020
Antioxidants/cell stress response						
25	Heat shock cognate 71 kDa protein	1,480 \pm 459	4,003 \pm 1,135	7,495 \pm 620	0.011	0.004
77	Glutathione S-transferase Mu 2	391 \pm 303	2,138 \pm 583	3,027 \pm 549	0.002	0.048
79	Catalase	475 \pm 409	1,113 \pm 235	1,908 \pm 444	0.035	0.046
83	Glutathione S-transferase P 1	685 \pm 332	1,422 \pm 71	3,027 \pm 635	0.005	0.006
84	Glutathione S-transferase Mu 1	384 \pm 204	4,466 \pm 303	6,020 \pm 839	0.001	0.047
102	Glutathione S-transferase A3	<DL	1,092 \pm 199	4,249 \pm 500	<0.001	<0.001

As compared to SSAT-wt, bold represents downregulation and bold italics means upregulation ($P < 0.05$, $n = 4$)

DL detection limit of SYPRO-Ruby fluorescent dye staining method

Author Manuscript

Author Manuscript

Author Manuscript

Author Manuscript

Table 2

Comparison of the proteomic data obtained from FSAT1KO, SSAT-ko and SSAT-tg mice

Protein list	FSAT1KO	SSAT-ko	SSAT-tg
Acyl-CoA-binding protein (ACBP)	<DL	0.47	0.57
α -Enolase	0.58	0.63	1.95
Carbonic anhydrase 3	0.65	0.38	1.33
Cytochrome c	0.71	0.37	1.23
Fructose-bisphosphate aldolase	<DL	0.56	1.47
Glutathione <i>S</i> -transferase class pi	0.71	0.48	2.13
Superoxide dismutase [Cu–Zn]	0.79	0.57	1.05
Vimentin	<DL	0.23	0.24
Adipocyte lipid-binding protein iodoacetamido-1,10-phenanthroline	<DL in WT group	3.92	0.86
Heat shock 70 kDa protein 1-like	<DL in WT group	2.85	0.50
L-Lactate dehydrogenase	1.46	6.19	<DL
Fatty acid-binding protein, adipocyte (AFABP)	1.47	1.71	0.94
Malate dehydrogenase (EC 1.1.1.37)	3.25	<DL	1.84

The data in the table indicates the fold change in protein quantity in FSAT1KO, SSAT-ko and SSAT-tg mice as compared with SSAT-wt mice. The bold font indicates downregulation as compared to SSAT-wt and bold italics font indicates upregulation as compared to SSAT-wt. Nine proteins [acyl-CoA binding protein, α -enolase, carbonic anhydrase 3, cytochrome c, fructose-bisphosphate aldolase, glutathione *S*-transferase class pi, superoxide dismutase (Cu–Zn), tubulin alpha chain isotype M-alpha-6, vimentin] were downregulated in both FSAT1KO and SSAT-ko mice comparing with SSAT-wt. Four proteins (adipocyte lipid-binding protein iodoacetamido-1,10-phenanthroline, heat shock 70 kDa protein 1-like, L-lactate dehydrogenase, fatty acid-binding protein, adipocyte) were upregulated in both FSAT1KO and SSAT-ko mice comparing with SSAT-wt. 1 protein (malate dehydrogenase) was upregulated in FSAT1KO and downregulated in SSAT-ko comparing with SSAT-wt